In situ evidence that mast cells release mutant NLRP1 in keratoacanthomas from multiple self-healing palmoplantar carcinoma

Alexandra Dobre[1,2], Tudor E. Fertig[1,3]*, Andrei M. Niculae[1,3,4], Adelina M. Cohn[1,5], Antoanela Curici[1,6], Razvan T. Andrei[6,7], Daciana S. Marta[3,8], Victor E. Peteu[3], Roua G. Popescu[9,10], George C. Marinescu[9,10], Gabriela Turcu[1,7,11], Ana M. Forsea[1,2,12], Daniela A. Ion[1], Mihaela Gherghiceanu[1,3]**, Roxana I. Nedelcu[1,11]**

[1] Carol Davila University of Medicine and Pharmacy, Bucharest, Romania

[2] Elias University Emergency Hospital, Dermatology, Bucharest, Romania

[3] Victor Babeş National Institute of Pathology, Bucharest, Romania

[4] Pathology Department, "Dr. Carol Davila" Central Military Emergency University Hospital, Bucharest, Romania

[5] Laboratoire National De Santé, Dudelange, Luxembourg

[6] Synevo Romania, Bucharest, Romania

[7] Colentina Clinical Hospital, Bucharest, Romania

[8] Faculty of Medicine, Titu Maiorescu University, Bucharest, Romania

[9] Asociația Independent Research, Bucharest, Romania

[10] Blue Screen SRL, Bucharest, Romania

[11] Derma 360 Clinic, Bucharest, Romania

[12] Health and Medical University Potsdam, Germany

*Corresponding author: Tudor Emanuel Fertig, +4021 319 2732, Dionisie Lupu 37, Bucharest 030167, emanuel.fertig@umfcd.ro

ABSTRACT

Multiple self-healing palmoplantar carcinoma (MSPC) is a rare syndrome characterized by germline mutations of the inflammasome sensor protein NLRP1, causing its constitutive activation and ultimately, IL1β-driven inflammation. Because NLRP1 is well expressed in human skin, the effect is aberrant keratinocyte proliferation with the appearance of characteristic, recurrent keratoacanthomas (KAs) on palms and soles. We aimed to clarify the subcellular localization of mutant NLRP1 in the skin of a MSPC patient with plantar KAs and a sudden psoriasis-like eruption. Skin biopsies from the MSPC patient and healthy controls were processed for immunohistochemistry and immunoelectron microscopy. We found for the first time that the protein NLRP1 localized to mast cell (MC) granules in both healthy and lesional skin. Moreover, MCs expressing the A66V pathogenic variant of NLRP1 overpopulated plantar KAs of a MSPC patient, infiltrated the epidermis and degranulated, a behavior not seen in the psoriasis-like lesion (PLL) from the same patient, nor in KAs from non-MSPC patients, nor healthy skin. The released granules had higher NLRP1 protein content than MSPC-PLL and also contained NLRP3 and IL1β. Overall, this data suggests that MCs can contribute to the pathogenesis of KAs in MSPC, which opens a new area of research in NLRP1-related syndromes.

41 **INTRODUCTION**

42 NLRP1 (NLR family pyrin domain containing 1) is a cytosolic sensor protein with a major role
43 in innate immunity. In response to pathogens or other stress signals, NLRP1 can participate in
44 the formation of an intracellular protein complex termed "inflammasome"[1], which allows
45 activation of caspase-1, followed by IL1β secretion and pyroptotic cell death[2].

46 In humans, NLRP1 pathogenic variants can lead to a variety of clinical syndromes depending
47 on the affected protein domain, mainly involving skin, cornea and lungs[3–6]. Multiple self-
48 healing palmoplantar carcinoma (MSPC) is an extremely rare such syndrome, characterized by
49 recurrent keratoacanthomas (KAs) that develop on palmoplantar skin and sporadically on other
50 epithelia lacking hair follicles[7]. Responsible are either one of three germline heterozygous
51 mutations (A54T, A66V, M77V) affecting the pyrin domain (PYD) of NLRP1, causing
52 spontaneous self-oligomerization of the protein, aberrant inflammasome activation and
53 subsequent proliferation of affected keratinocytes[7].

54 Keratinocytes are known as the main NLRP1 reservoir in human skin[7–10], however
55 granulocytes, lymphocytes, macrophages and dendritic cells also express NLRP1[11]. RNA-seq
56 data from the Human Protein Atlas indicates basophils as having the highest potential for
57 NLRP1 protein expression among immune cells[12,13].

58 Mast cells (MCs) are tissue-resident immune cells of hematopoietic origin, which differentiate
59 from a basophil-MC common progenitor. Although not yet described to contain NLRP1, MCs
60 contain NLRP3 within secretory granules and are capable of producing IL1β following NLRP3
61 inflammasome activation[14,15]. Mutations of NLRP3 cause it to become constitutively activated
62 in MCs, initiating overproduction of IL1β. In humans, this contributes to a spectrum of clinical
63 entities named cryopyrin-associated periodic syndromes (CAPS), in which the skin, joints and
64 central nervous system can be affected[14,16].

65 We report for the first time that skin MCs harbor NLRP1 within granules. We further show
66 massive and specific degranulation of MCs in different KAs of a MSPC patient with
67 $NLRP1^{A66V}$ and suggest that release of granules containing this hyperactive NLRP1 variant
68 contributes to the pathogenesis of KAs in this syndrome.

MATERIALS & METHODS

Patients and samples

All subjects gave written informed consent prior to biopsy. Four samples were collected from a single MSPC patient with NLRP1^{A66V}: three different KAs from plantar regions (in 2016, 2023 and 2025) and a sample from a psoriasis-like plaque on the abdomen (in 2023). Biopsies were collected from the elbow region of two clinically healthy volunteers. The study included 6 archived formalin-fixed paraffin-embedded (FFPE) KA specimens, from different patients with no clinical history of MSPC. A human lymph node FFPE specimen was included as NLRP1 positive control. This study was performed in conformity with the Declaration of Helsinki and received approval from the ethics committees at Victor Babeș National Institute of Pathology and Elias University Emergency Hospital, Bucharest, Romania.

Light microscopy and immunohistochemistry

Hematoxylin-eosin was done by routine protocol. IHC with the primary antibody of interest (**Table S1**) was done using an Autostainer Link 48, following manufacturer specifications (Dako, Agilent Technology, US). An isotype control and omission of primary antibody were used to verify non-specific binding. Digital slides were generated using an automated slide scanner (Aperio AT2, Leica Biosystems, US).

Immunoelectron microscopy

Biopsies were fixed in a solution comprising 4% paraformaldehyde, 0.5% glutaraldehyde, and 1.4% sucrose (pH 7.4), then embedded in London Resin White (LR White, Agar Scientific, UK). Ultra-thin sections were mounted on formvar and carbon-coated nickel grids, then incubated with the primary antibody of interest (**Table S1**) and a gold-conjugated secondary antibody at 1:50 dilution (Aurion, The Netherlands). Negative controls had primary antibodies

92 omitted and an isotype control was used to exclude nonspecific binding to MC Fc receptors. A
93 blocking solution for goat antibodies was used to reduce nonspecific binding (Aurion, The
94 Netherlands). Imaging was done using a 4×4k Ceta camera, on a Talos 200C transmission
95 electron microscope (Thermo Fisher Scientific, US).

96 **Immunoelectron tomography**

97 This method allowed simultaneous labeling with up to three different primary antibodies.
98 Briefly, LR White sections (300 nm) were adhered to nickel grids precoated with 0.01% poly-
99 L-lysine and without formvar or carbon. For double-labeling, grids were incubated on each
100 side, consecutively, with two primary antibodies raised in different species (mouse and rabbit,
101 **Table S1**). For triple-labeling, grids were incubated on one side with a mixture of two
102 antibodies raised in different species (mouse and rabbit, **Table S1**), then either a rabbit or
103 mouse primary antibody was used on the other side. To facilitate identification, secondary
104 antibodies had different colloidal gold diameters for each target (6, 10 and 15 nm, Aurion, The
105 Netherlands). Absence of cross-contamination between section faces was verified by
106 immunolabeling control grids on one side, while the other side was incubated with PBS.
107 Acquisition of single axis tilt series and tomographical reconstruction and segmentation in
108 IMOD-eTomo[17], were done as described elsewhere[18].

109 **Data analysis**

110 Quantification of MCs was performed on tissue sections stained for tryptase. For each case,
111 tryptase-positive cells were manually counted in ten consecutive high-power fields (HPF, 40×
112 objective), starting from a hotspot. Each experimental group included approximately 27
113 observations ($n \approx 27$ per group). To quantify the NLRP1 content of MC granules, cells were
114 first identified on randomly selected ultrathin sections from the MSPC and healthy skin
115 specimens, immunolabeled under identical conditions. Entire MCs were imaged, then colloidal

gold was counted on all granules of each cell. Each experimental group included approximately 1,058 observations ($n \approx 1{,}058$ per group).

Statistical analyses were performed using one-way ANOVA, followed by Tukey's post hoc test for pairwise comparisons between groups. Statistical significance is presented only for comparisons with p-values $< .05$. The post hoc statistical power for the applied tests was 1. All analyses and graphical representations were generated using R software (version 4.4.1).

122 **RESULTS**

123 **MSPC patient develops overlapping psoriasis-like skin condition**

124 A 49-year-old male with a history of multiple central hyperkeratotic lesions on the palms and
125 soles (**Figure 1a**) in the context of a previously diagnosed MSPC with the A66V pathogenic
126 variant of NLRP1[7], presented with symmetrically distributed and well-defined erythematous-
127 squamous plaques, some with erosions and crusting. These initially appeared on the dorsal feet
128 and later spread to the extremities, trunk and head (**Figure 1b**). An infection was ruled out
129 because of unresponsiveness to antibiotics/antifungals. Instead, an overlap of allergic contact
130 dermatitis with psoriasis was suspected due to: (a) histopathological diagnosis of psoriasis on
131 an abdominal plaque (**Figure 1c**), (b) atypical development and clinical presentation of
132 plaques, (c) positive patch-tests to lanolin alcohol and nickel(II) sulfate hexahydrate, (d) good
133 response of lesions to oral corticotherapy and lanolin-free moisturizers, (e) IgE approximately
134 twice the normal value at presentation, which normalized after treatment, and (f) no recurrence
135 after corticotherapy.

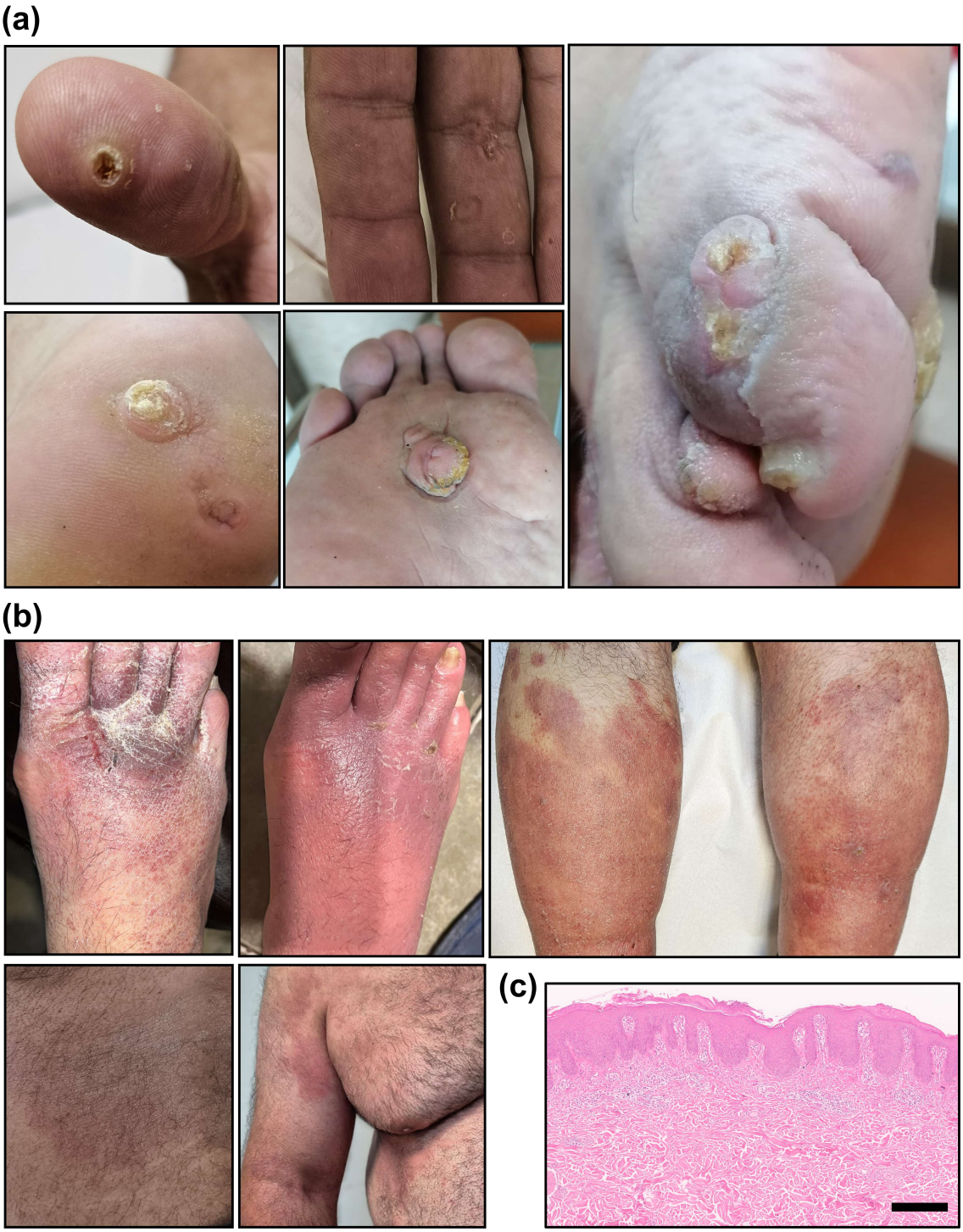

136

137 **Figure 1. Clinical features of a patient with multiple self-healing palmoplantar carcinoma**
138 **(MSPC). (a)** Keratoacanthomas at different stages of evolution on the palmar and plantar
139 surfaces. **(b)** Sudden development of poorly-defined erythemato-edematous plaques with
140 erosions and scales on the dorsal feet. This evolved to a widespread eruption of well-defined
141 erythemato-squamous plaques, including on the lower limbs and trunk. Some plaques
142 resembled psoriasis. **(c)** Light microscopy (HE) of abdominal lesion from MSPC patient,
143 showing relatively thin suprapapillary epidermis, psoriasiform epidermal hyperplasia with
144 focal parakeratosis and hypogranulosis. There are neutrophil collections in the mounds of
145 parakeratosis and moderate perivascular lymphocytic infiltrate in the superficial dermis.
146 Images are published with patient consent. Scale bar = 300 µm.

147 **Degranulating MCs accumulate in MSPC-KAs**

148 Given that the psoriasis-like lesions (PLL) appeared in a patient with MSPC, we aimed to
149 understand how the lesional microenvironment and subcellular distribution of NLRP1^{A66V}
150 differed when compared to three plantar KAs from the same patient (biopsied 7 years prior,
151 concomitantly and 2 years after MSPC-PLL diagnosis) and to wild-type NLRP1 in the skin
152 from a healthy control.

153 First, we confirmed the presence of NLRP1 by mass spectrometry, in all samples, as identified
154 by at least two tryptic peptides having at least 2 transitions (MS2, resulted by collision induced
155 dissociation) (**Figure S1, Table S2**).

156 Then, we used immunohistochemistry (IHC) to look at the tissue distribution of NLRP1^{A66V} in
157 the three MSPC-KAs. As reported[7], keratinocytes were positive for NLRP1, with a nucleo-
158 cytoplasmic staining pattern and the intensity gradually decreasing towards the upper
159 epidermal layers (**Figure 2a**). Unexpectedly however, NLRP1 staining was more intense in the
160 dermis than the epidermis, with specific cell populations presenting a granular distribution
161 within the cytoplasm (**Figure 2a, top row inset**). Inversely, NLRP1^{A66V} expression was highest
162 in the epidermis of the MSPC-PLL sample, but comparatively reduced in the dermis, mainly
163 clustering around blood vessels (**Figure 2a**). Healthy skin showed the least NLRP1 staining
164 intensity in both epidermis and dermis (**Figure 2a**), although the granular distribution persisted
165 in cells surrounding blood vessels. Staining of immune cell granules by NLRP1 was confirmed
166 on a human lymph node specimen (**Figure S2a**), whereas the isotype control did not bind
167 (**Figure 2a**).

168 To investigate whether some of the numerous NLRP1-positive cells in the MSPC-KA dermis
169 were MCs, we stained using tryptase and CD117/c-kit (**Figure 2a**). Indeed, KA samples from
170 the MSPC patient had significant MC accumulation (27.2/mm^2), above MSPC-PLL

171 (17.5/mm^2) or healthy skin (7.6/mm^2) (**Figure 2b**). In MSPC-KAs but not MSPC-PLL, MCs
172 frequently infiltrated epidermal layers (**Figure 2a, second row inset**).
173 Under higher magnification we further observed that MCs in MSPC-KAs, but not MSPC-PLL,
174 were degranulated. Tryptase-positive granular material was widely distributed within
175 connective tissue and taken up in the epidermis, up to and including the spinous layer (**Figure**
176 **2c**).
177 To verify if this is a characteristic of all KAs or if this was restricted to the three MSPC-KAs
178 in this study, we used tryptase staining on six KAs from patients not diagnosed with MSPC
179 (**Figure S2b**). As expected[19], these presented MCs in higher numbers (13/mm^2) than healthy
180 skin, however below counts in MSPC-KAs and even MSPC-PLL (**Figure 2b**). Importantly, we
181 could not identify MC epidermal infiltration, nor significant MC degranulation, indicating their
182 distinct contribution in MSPC-KA pathogenesis.
183 The MSPC patient was negative for the D816V KIT pathogenic variant in whole blood and had
184 normal serum tryptase (<11.4 µg/L), limiting the possibility of MC neoplastic transformation.

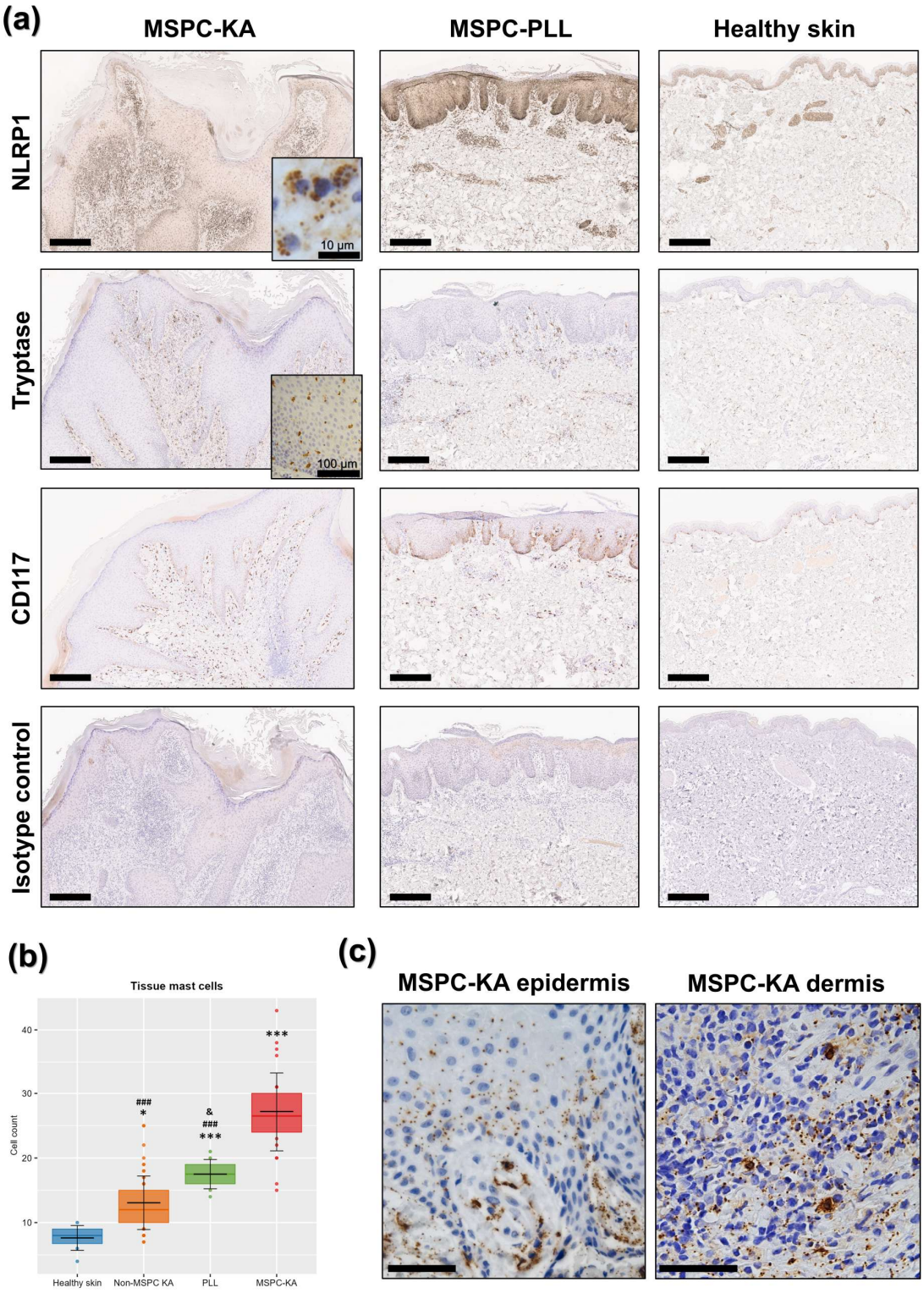
(a)
MSPC-KA
MSPC-PLL
Healthy skin
NLRP1
Tryptase
CD117
Isotype control
10 µm
100 µm
(b)
Tissue mast cells
Cell count
40
30
20
10
Healthy skin
Non-MSPC KA
PLL
MSPC-KA
###
*
&
###
***
***
(c)
MSPC-KA epidermis
MSPC-KA dermis

185

186 **Figure 2. Immunohistochemistry of keratoacanthomas (KAs) in multiple self-healing**
187 **palmoplantar carcinoma (MSPC). (a)** In MSPC-KAs, NLRP1^{A66V} was more highly
188 expressed in the dermis and was concentrated in cell granules **(top row inset**, scale bar = 10
189 µm**)**. In the psoriasis-like lesion (MSPC-PLL), NLRP1^{A66V} was overrepresented in the
190 epidermis. CD117 and tryptase staining demonstrated more mast cells (MCs) in MSPC-KAs,
191 including epidermal infiltration **(second row inset,** scale bar = 100 µm**)**. Scale bars = 300 µm.
192 **(b)** Quantification of MCs in the analysed samples, presented as means ± standard deviation
193 (SD). Statistical significance is shown against healthy skin—*, MSPC-KA group—#, and the
194 non-MSPC KA group—&, where */& $p < .05$; ***/### $p < .001$. **(c)** MCs in MSPC-KAs were
195 degranulated, with granular material dispersed in epidermis and dermis. Scale bars = 50 µm.

196 **NLRP1 localizes to MC granules**

197 For more precise subcellular localization of NLRP1 we employed IEM. Morphologically, most
198 MCs from MSPC-KA were degranulated, ranging from having empty granules and granules
199 fused with the plasma membrane, to complete fragmentation of cells, with release of clumps
200 of granular complexes in the extracellular space (**Figure 3a**). By contrast, MCs from MSPC-
201 PLL and healthy skin had typical appearance (intact granule architecture, presence of plasma
202 membrane folds) and localized in proximity of blood vessels (**Figure 3b,c**).

203 Using two different, commercially available anti-NLRP1 antibodies, we demonstrated that
204 NLRP1 accumulates in granules of MCs from both lesional and healthy skin, regardless of
205 granule morphology and degranulation status of the cell, indicating NLRP1 is a ubiquitous
206 component of skin MCs (**Figure 3a,c and inset**). By contrast, an isotype control did not bind
207 (**Supplementary Figure 3a**). Next, we asked whether there are differences in MC NLRP1
208 content between samples, so we manually counted and averaged colloidal gold per granule,
209 under identical immunolabeling conditions. In this context, this method of quantification was
210 preferred to mass spectrometry of tissue lysates, as it measured protein content in the
211 subcellular compartment of interest, unbiased by overall density of MCs in tissue. We found
212 that NLRP1^{A66V} from MSPC-KA was overrepresented compared to NLRP1^{A66V} in MSPC-PLL
213 or wild-type NLRP1 in healthy skin (**Figure 3d**), further suggesting MCs may serve as a
214 reservoir of hyper-reactive NLRP1^{A66V} during MSPC-KA pathogenesis. Interestingly, MC
215 granules in MSPC-PLL had lower NLRP1 content than healthy skin, although the significance
216 of this is unclear.

217 In accordance with IHC, NLRP1 was also localized in keratinocytes in all samples, however it
218 unexpectedly clustered around intermediate filaments and desmosomes (**Figure S3b**).

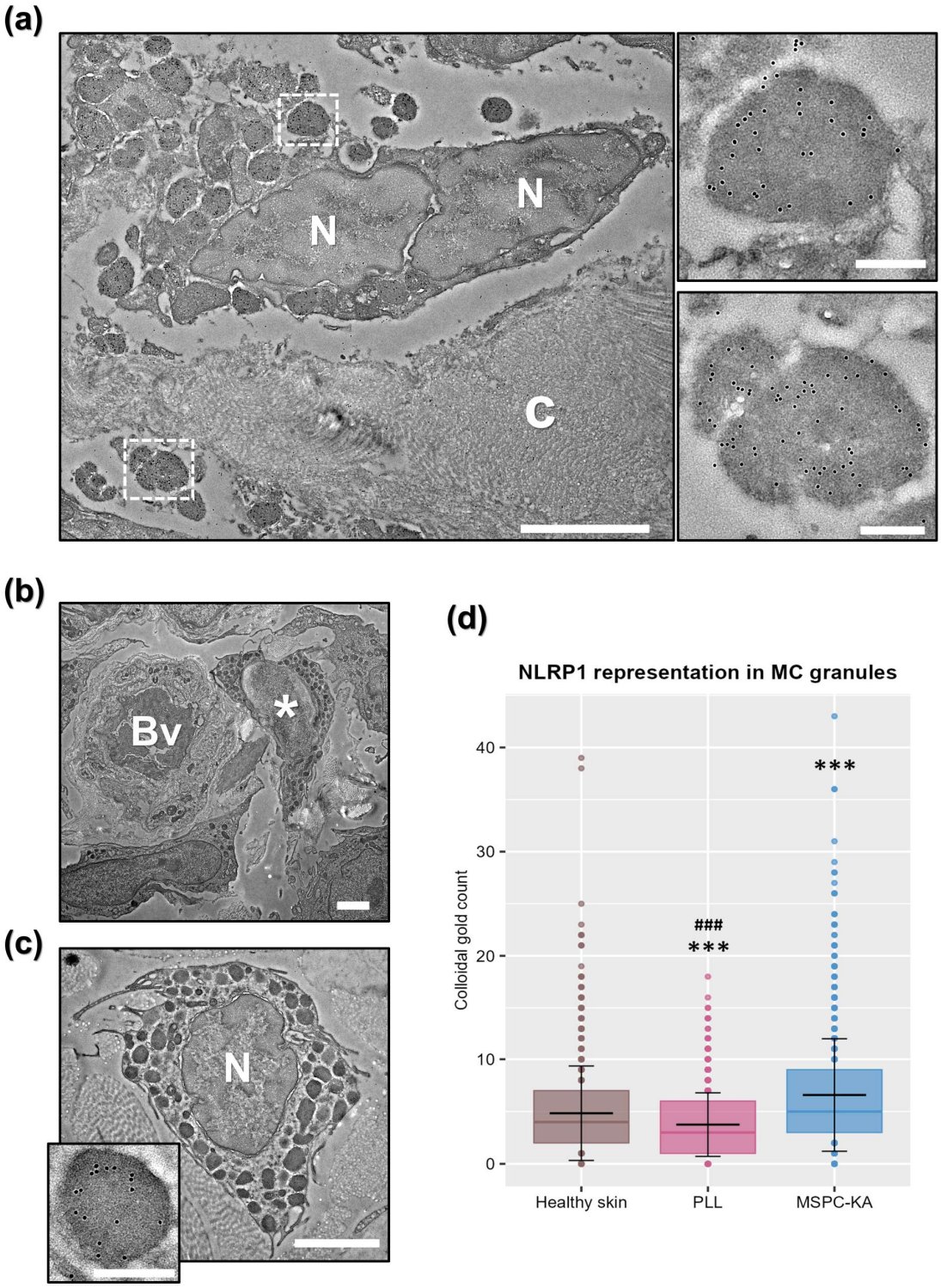
(a)
N
N
C
(b)
Bv
*
(c)
N
(d)
NLRP1 representation in MC granules
Colloidal gold count
40
30
20
10
0
***
###
***
Healthy skin
PLL
MSPC-KA

219

220 **Figure 3. NLRP1 is ubiquitous in skin mast cell (MC) granules. (a)** MCs in
221 keratoacanthomas (KAs) from a multiple self-healing palmoplantar carcinoma (MSPC) patient
222 were degranulated. Scale bar = 2 µm. *c - collagen, N - nucleus.* MC granules in MSPC-KA
223 presented $NLRP1^{A66V}$ accumulation, as exemplified by higher magnifications of boxed areas.
224 Gold labeling is seen as black dots. Scale bars = 250 nm. **(b)** MCs from a psoriasis-like lesion
225 (MSPC-PLL) were morphologically normal (*) and clustered around blood vessels (Bv). Scale
226 bar = 2 µm. **(c)** Normal MC in healthy skin presenting NLRP1 in granules **(inset**, scale bar =
227 250 nm**)**. Scale bar = 2 µm. **(d)** Quantification of colloidal gold demonstrated MCs in MSPC-
228 KA had more NLRP1 (means ± standard deviation). Statistical significance is shown against
229 healthy skin—*, and MSPC-KA—#, where ***/### $p < .001$.

230 **NLRP1 and NLRP3 can colocalize in MC granules**

231 MCs are known to contain all components of the NLRP3 inflammasome and to secrete IL1β in
232 a NLRP3-dependent manner[14,15]. Given our finding that NLRP1^{A66V} was present in MC
233 granules from the MSPC patient, we were curious whether it spatially overlapped with NLRP3
234 and if it could therefore share elements of the inflammasome machinery during activation.
235 First, we labeled MSPC-KA against pro-IL1β/IL1β (hereafter IL1β) and found it well
236 represented in both intracellular MC granules and in MC-derived extracellular granular
237 material **(Figure 4a and inset)**. This demonstrated that MCs in MSPC-KA secrete this pro-
238 inflammatory cytokine in the extracellular space during degranulation.

239 Next, we confirmed that some MC granules also contained NLRP3 **(Figure 4b and inset)** and
240 released it during degranulation. NLRP3 was frequently localized at the periphery of
241 cytoplasmic granules and at the plasma membrane in degranulating MCs **(Figure 4b)**, in
242 agreement with a recently published study showing a role for NLRP3 in granule exocytosis[20].
243 Electron tomography on double-labeled sections revealed that NLRP1 and NLRP3 can
244 colocalize to some, but not all MC granules **(Figure S3c-e, Movie S1)**. This raises the
245 possibility of compartimentalisation of inflammasome pathways within MCs, but further
246 clarification was impossible due to variations in labeling efficiencies between the different
247 primary and secondary antibodies used. Finally, triple-labeling revealed that both sensor
248 proteins can colocalize with IL1β, in both intra- and extracellular MC granules **(Figure 4c-e,**
249 **Movie S2)**.

250 Taken together, these findings confirm that multiple inflammasome sensor proteins can
251 simultaneously inhabit MC granules and consequently may act in tandem during activation of
252 MCs in MSPC-KAs.

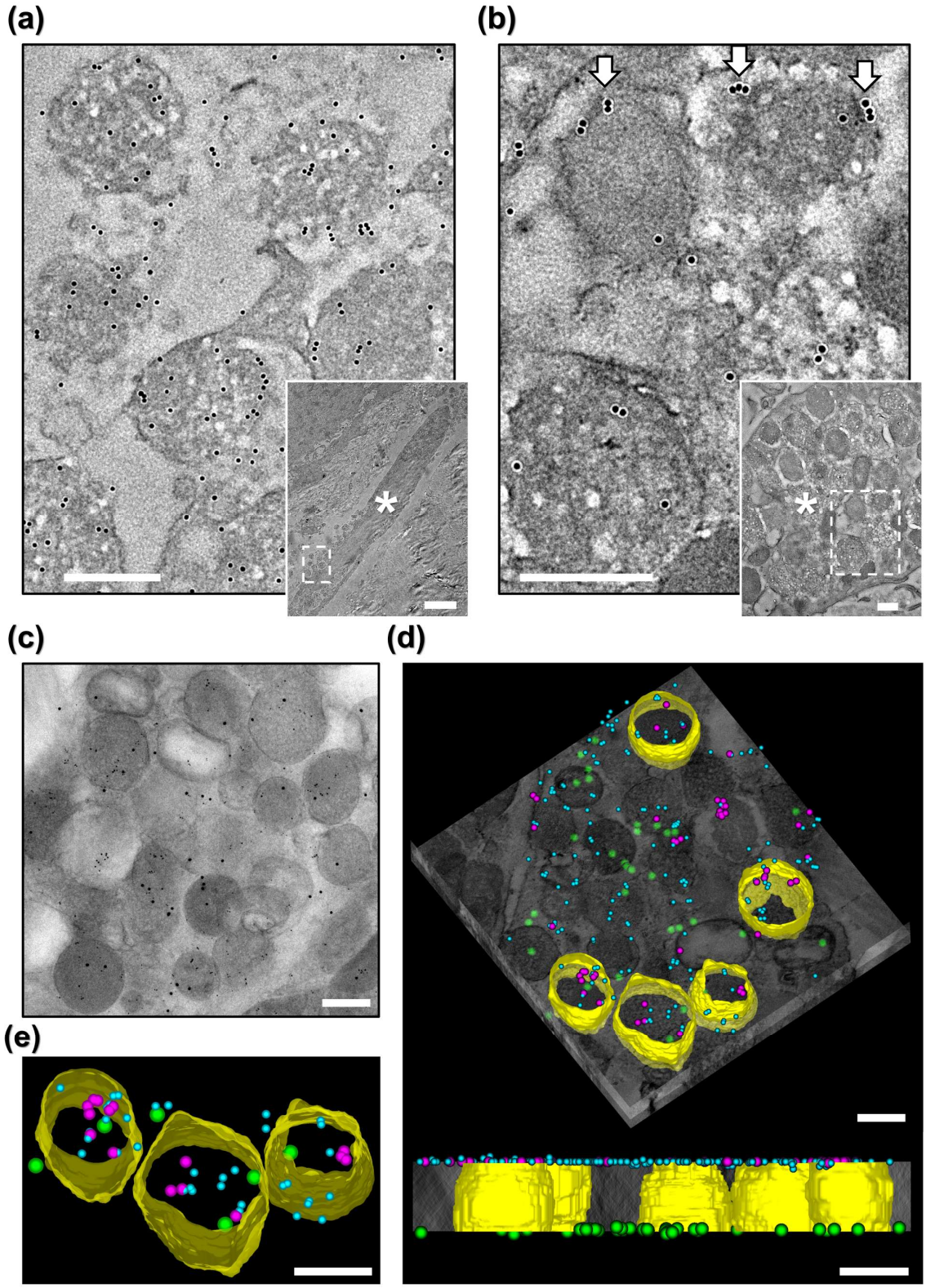

253

254 **Figure 4. NLRP1^{A66V}, NLRP3 and IL1β colocalize to mast cell (MC) granules in a MSPC-**
255 **keratoacanthoma. (a)** High magnification of box in inset, confirming pro-IL1β/IL1β in
256 granular material released by a MC (*). **(b)** High magnification of box in inset, showing MCs
257 (*) contain NLRP3, which frequently localized to the periphery of granules (arrows). **(c)**
258 Projection from tomographic tilt series, showing colocalization of gold labels (NLRP1^{A66V},
259 NLRP3, IL1β) in MC granules. **(d, top)** Reconstructed tomogram with superimposed contours
260 of five MC granules (yellow), presenting colocalization of NLRP1^{A66V} (magenta), NLRP3
261 (turquoise) and IL1β (green). **(d, bottom)** Side-view showing distribution of labels to each side
262 of the imaged resin section. **(e)** Detail of segmented MC granules. Scale bar for inset (a) = 2.5
263 µm, all others = 300 nm.

264 **DISCUSSION**

265 Here, we demonstrated that skin MCs can act as a reservoir for NLRP1, a critical but less
266 known inflammasome sensor protein. Although novel, this finding is not completely surprising,
267 as MCs express pattern recognition receptors and harbor all components of the NLRP3
268 inflammasome pathway[15], some of which are also required for NLRP1 inflammasome
269 assembly.

270 We next showed that MCs are directly involved in the pathogenesis of KAs in a MSPC patient
271 with NLRP1^{A66V}. In three different plantar lesions, temporally separated from initial diagnosis
272 by 1, 8 and 10 years, MCs infiltrated the epidermis and NLRP1^{A66V} was released in the dermis
273 and epidermis through widespread MC degranulation.

274 KAs in MSPC develop as a consequence of pathological inflammasome activation in select
275 keratinocytes, due to mutation-induced ablation of NLRP1 auto-inhibition[7]. The fact that this
276 process is absent in hair-bearing skin despite ubiquitous skin distribution of mutant NLRP1
277 indicates highly specific triggers within the palmoplantar skin microenvironment. In our
278 samples, MC behaviour was also different between skin types. Whereas the plantar KAs
279 presented very high numbers of degranulated MCs which infiltrated the epidermis, these
280 features were conspicuously absent in a PLL lesion from the abdominal skin of the same MSPC
281 patient and also absent in KAs from 6 non-MSPC patients.

282 One possibility is that the pathological activation of MCs in MSPC-KAs is a response to
283 NLRP1-driven inflammasome activation in local keratinocytes and subsequent release of pro-
284 inflammatory factors. However, this is difficult to reconcile with two key findings: (1) that the
285 highest intensity of NLRP1 staining was in the MSPC-PLL epidermis, where keratinocytes
286 also express the hyperactive NLRP1^{A66V}, yet do not form KAs, and (2) that compared to healthy

287 skin, MSPC-PLL presented high numbers of MCs prone to activation by local keratinocyte
288 inflammatory cues, but these MCs had normal morphology.

289 Instead, the particular MC behaviour in the plantar skin of this MSPC patient may be the result
290 of intrinsic NLRP1-inflammasome activation in response to yet unknown triggers, possibly
291 microbial stimuli or local IgE secretion[21]. Activation of select MC clusters and release of
292 granular material would induce keratinocyte inflammatory responses, in turn driving more
293 extensive MC recruitment within the lesion (**Figure 5**).

294 In support of this, we showed that MC granular material was widely spread throughout the
295 basal and spinous layers of MSPC-KAs. These granules had higher NLRP1 content than
296 equivalents in MSPC-PLL and healthy skin and harbored NLRP3 and the pro-inflammatory
297 cytokine IL1β. The latter can be converted to its active form within intact granules via the
298 NLRP1 and NLRP3 inflammasome pathways, but also in the extracellular environment by
299 various endogenous proteases[20,22]. Regardless of the mechanism of activation, the diffusion of
300 extracellular IL1β from widespread MC degranulation could stimulate keratinocyte
301 proliferation[22]. Additionally, tryptase released during MC degranulation can cleave protease
302 activated receptor 2 (PAR-2) on the surface of keratinocytes[23], a process which stimulates non-
303 specific particle uptake through endocytosis[24]. In MSPC-KAs, this would allow enrichment of
304 keratinocytes with components of the NLRP1/NLRP3 inflammasome pathways. Even in the
305 absence of uptake of inflammasome components, other MC granule contents, like histamine,
306 serotonin and keratinocyte growth factor, are known to stimulate keratinocyte proliferation *in*
307 *situ* in mice and in human cell cultures[25,26]. The characteristic palmoplantar epidermal
308 hyperplasia in MSPC-KAs may therefore be conditioned by aberrant, NLRP1-dependent
309 activity of tissue-resident MCs.

310 This study has two important limitations. First, in absence of functional studies, we cannot
311 definitively ascertain whether MC degranulation is a prerequisite for MSPC-KA formation, or
312 if it is a local response mechanism which merely modulates lesion development. As murine
313 NLRP1 lacks the PYD domain[7], an *in vitro* experiment would be required, involving co-culture
314 of human keratinocytes with MCs expressing mutant NLRP1. Second, because we could only
315 include a single MSPC patient, carrying the $NLRP1^{A66V}$ pathogenic variant, we are unable to
316 extrapolate our findings to other MSPC variants, or generally to syndromes caused by NLRP1
317 mutations. This is further hindered by the rarity of these diseases, with only 5 MSPC families
318 known worldwide[27].
319 In summary, we showed for the first time that NLRP1 is a component of skin MC granules and
320 can colocalize with NLRP3 and IL1β, indicating that MCs have more avenues for
321 inflammasome activation than previously known. We also showed that when MCs from plantar
322 skin express $NLRP1^{A66V}$, they proliferate, infiltrate the epidermis and degranulate, contributing
323 to the pathogenesis of KAs in this variant of MSPC. This opens a new area of research in
324 NLRP1-related syndromes and, if confirmed in other patients, would translate clinically to
325 accessible therapies targeting MC activity.

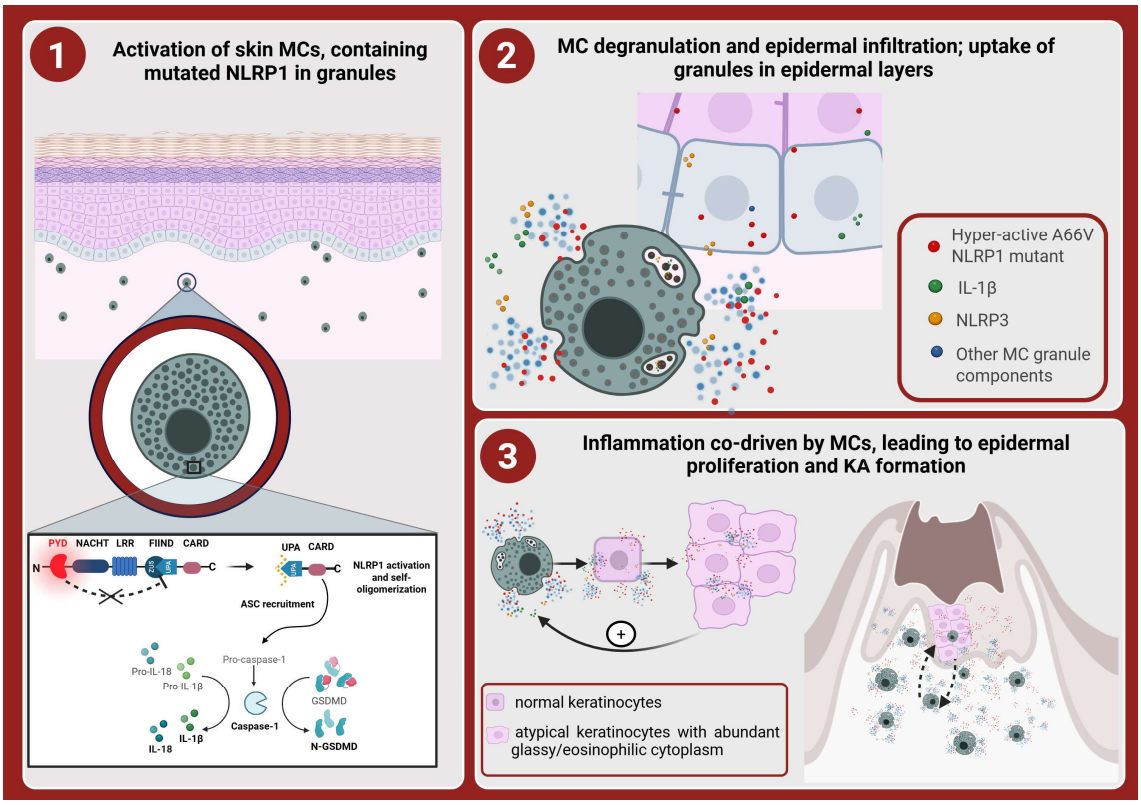

Figure 5. Potential mast cell (MC) involvement in keratoacanthoma (KA) formation in multiple self-healing palmoplantar carcinoma. MCs expressing NLRP1^{A66V} proliferate and become activated in the dermis, stimulated by an unknown mechanism, possibly IL1β secretion by keratinocytes **(1)**. Constitutive activation of the NLRP1 inflammasome **(1 - inset)** leads to catastrophic degranulation of MCs. Granular material containing inflammasome components is taken up by keratinocytes up to the spinous layer **(2).** This leads to further inflammatory responses in keratinocytes and initiates a feedback loop driving activation of more MCs, which also infiltrate the lesion. Persistent inflammation induces keratinocyte hyperplasia and KA development **(3)**.

Ethics statement. The study was performed in accordance with the Declaration of Helsinki and was approved by Victor Babeș National Institute of Pathology (117/12.12.2023) and Elias University Emergency Hospital, Bucharest, Romania (122052024-2/22.05.2024). All participants provided written informed consent to participate in this study.

Data availability statement. Immunohistochemistry and transmission electron microscopy data other than presented in the article can be shared on reasonable request to the corresponding author.

Conflict of interest. The authors declare that they have no conflicts of interest.

Acknowledgments: We are grateful to the MSPC patient for participating in this study. The graphical abstract and Figure 5 were created with BioRender.com. Publication of this paper was supported by the University of Medicine and Pharmacy Carol Davila, through the institutional program Publish not Perish.

Funding: This work was supported by the Ministry of Research, Innovation and Digitalization, CCCDI - UEFISCDI, project number PN-IV-P7-7.1-PED-2024-0814, within PNCDI IV and through the National Research Authority Core Program PN-10N/2023-23.16.01.01.

Contributor statement. Conceptualization: A.D., T.E.F., R.G.P., G.C.M., D.A.I., M.G. and R.I.N.**; Data Curation:** A.D. and T.E.F.,**; Formal Analysis:** R.G.P., G.C.M., A.D., T.E.F. and A.M.C.**; Funding Acquisition:** M.G., D.A.I., G.C.M., G.T., R.I.N. and A.C.**; Investigation:** A.D., T.E.F., A.M.N., A.M.C. and R.T.A.**; Methodology:** T.E.F., A.M.N., V.E.P, D.S.M. and M.G.**; Project Administration:** T.E.F.**; Resources:** R.I.N., A.M.C. and A.M.F.**; Supervision:** A.M.F., D.A.I., M.G. and R.I.N**; Validation:** All authors**; Visualization:** A.D. and T.E.F.**; Writing – Original Draft Preparation:** A.D. and T.E.F.**; Writing – Review & Editing:** All authors**.**

359 **REFERENCES**

360 1. Martinon F, Burns K, Tschopp J. The Inflammasome: A molecular platform triggering
361 activation of inflammatory caspases and processing of proIL-β. Mol Cell [Internet]. 2002 [cited
362 2025 Jun 21];10:417–26. Available from: https://pubmed.ncbi.nlm.nih.gov/12191486/
363 2. Bauernfried S, Hornung V. Human NLRP1: From the shadows to center stage. Journal of
364 Experimental Medicine [Internet]. 2021 [cited 2025 Jun 21];219. Available from:
365 https://doi.org/10.1084/jem.20211405
366 3. Barry K, Murphy C, Mansell A. NLRP1- A CINDERELLA STORY: a perspective of recent
367 advances in NLRP1 and the questions they raise. Commun Biol [Internet]. 2023 [cited 2025
368 Jun 21];6:1–7. Available from: https://www.nature.com/articles/s42003-023-05684-3
369 4. Mitchell PS, Sandstrom A, Vance RE. The NLRP1 inflammasome: new mechanistic
370 insights and unresolved mysteries. Curr Opin Immunol [Internet]. 2019 [cited 2025 Jun
371 21];60:37–45. Available from: https://pubmed.ncbi.nlm.nih.gov/31121538/
372 5. Burian M, Schmidt MF, Yazdi AS. The NLRP1 inflammasome in skin diseases. Front
373 Immunol. 2023;14:1111611.
374 6. Calabrese L, Fiocco Z, Mellett M, Aoki R, Rubegni P, et al. Role of the NLRP1
375 inflammasome in skin cancer and inflammatory skin diseases. British Journal of Dermatology
376 [Internet]. 2024 [cited 2025 Jun 21];190:305–15. Available from:
377 https://pubmed.ncbi.nlm.nih.gov/37889986/
378 7. Zhong FL, Mamaı¨, M, Sborgi L, Saad A, Hiller S, et al. Germline NLRP1 Mutations Cause
379 Skin Inflammatory and Cancer Susceptibility Syndromes via Inflammasome Activation. Cell
380 [Internet]. 2016 [cited 2024 Apr 18];167:187–202. Available from:
381 http://dx.doi.org/10.1016/j.cell.2016.09.001
382 8. Sand J, Haertel E, Biedermann T, Contassot E, Reichmann E, et al. Expression of
383 inflammasome proteins and inflammasome activation occurs in human, but not in murine
384 keratinocytes. Cell Death Dis [Internet]. 2018 [cited 2025 Jun 21];9:1–14. Available from:
385 https://www.nature.com/articles/s41419-017-0009-4
386 9. Feldmeyer L, Keller M, Niklaus G, Hohl D, Werner S, Beer HD. The Inflammasome
387 Mediates UVB-Induced Activation and Secretion of Interleukin-1β by Keratinocytes. Current
388 Biology [Internet]. 2007 [cited 2025 Jun 21];17:1140–5. Available from:
389 https://www.sciencedirect.com/science/article/pii/S0960982207015084

390 10. Marie J, Kovacs D, Pain C, Jouary T, Cota C, et al. Inflammasome activation and
391 vitiligo/nonsegmental vitiligo progression. Br J Dermatol. 2014 Apr;170(4):816-23. doi:
392 10.1111/bjd.12691. PMID: 24734946.
393 11. Kummer JA, Broekhuizen R, Everett H, Agostini L, Kuijk L, et al. Inflammasome
394 components NALP 1 and 3 show distinct but separate expression profiles in human tissues
395 suggesting a site-specific role in the inflammatory response. Journal of Histochemistry and
396 Cytochemistry [Internet]. 2007 [cited 2025 Jun 21];55:443–52. Available from:
397 https://pubmed.ncbi.nlm.nih.gov/17164409/
398 12. Karlsson M, Zhang C, Méar L, Zhong W, Digre A, et al. A single–cell type
399 transcriptomics map of human tissues. Sci Adv [Internet]. 2021 [cited 2025 Jun 21];7.
400 Available from: https://pubmed.ncbi.nlm.nih.gov/34321199/
401 13. The Human Protein Atlas [Internet]. [cited 2025 Jun 21]. Available from:
402 www.proteinatlas.org
403 14. Nakamura Y, Kambe N, Saito M, Nishikomori R, Kim YG, et al. Mast cells mediate
404 neutrophil recruitment and vascular leakage through the NLRP3 inflammasome in histamine-
405 independent urticaria. Journal of Experimental Medicine [Internet]. 2009 [cited 2025 Jul
406 16];206:1037–46. Available from: https://pubmed.ncbi.nlm.nih.gov/19364881/
407 15. Bonnekoh H, Scheffel J, Kambe N, Krause K. The role of mast cells in
408 autoinflammation. Immunol Rev [Internet]. 2018 [cited 2025 Apr 22];282:265–75. Available
409 from: https://pubmed.ncbi.nlm.nih.gov/29431217/
410 16. Nakamura Y, Franchi L, Kambe N, Meng G, Strober W, Núñez G. Critical Role for
411 Mast Cells in Interleukin-1β-Driven Skin Inflammation Associated with an Activating
412 Mutation in the Nlrp3 Protein. Immunity [Internet]. 2012 [cited 2025 Jun 21];37:85–95.
413 Available from: https://pubmed.ncbi.nlm.nih.gov/22819042/
414 17. Kremer JR, Mastronarde DN, McIntosh JR. Computer visualization of three-
415 dimensional image data using IMOD. Journal of Structural Biology. 1996 Jan-Feb;116(1):71-
416 76. DOI: 10.1006/jsbi.1996.0013. PMID: 8742726.
417 18. Ceafalan LC, Fertig TE, Gheorghe TC, Hinescu ME, Popescu BO, et al. Age-related
418 ultrastructural changes of the basement membrane in the mouse blood-brain barrier. J Cell Mol
419 Med [Internet]. 2019 [cited 2025 Jul 16];23:819–27. Available from:
420 https://pubmed.ncbi.nlm.nih.gov/30450815/
421 19. Aguiar ALM, Martins CJ, Meuser-Batista M, Carvalho V, Barreto EO, et al. A case of
422 keratoacanthoma centrifugum marginatum with a curious mast cell accumulation at tumour

423 sites [28]. Journal of the European Academy of Dermatology and Venereology [Internet]. 2007
424 [cited 2025 Apr 26];21:429–31. Available from: https://pubmed.ncbi.nlm.nih.gov/17309493/
425 20. Mencarelli, A., Bist, P., Choi, H.W. *et al.* Anaphylactic degranulation by mast cells
426 requires the mobilization of inflammasome components. *Nat Immunol* 25, 693–702 (2024).
427 https://doi.org/10.1038/s41590-024-01788-y
428 21. Galli, S., Tsai, M. IgE and mast cells in allergic disease. *Nat Med* **18**, 693–704 (2012).
429 https://doi.org/10.1038/nm.2755
430 22. Macleod T, Berekmeri A, Bridgewood C, Stacey M, McGonagle D, Wittmann M. The
431 Immunological Impact of IL-1 Family Cytokines on the Epidermal Barrier. Front Immunol
432 [Internet]. 2021 [cited 2025 Jul 16];12:808012. Available from: www.frontiersin.org
433 23. Santulli RJ, Derian CK, Darrow AL, Tomko KA, Eckardt AJ, et al. Evidence for the
434 presence of a protease-activated receptor distinct from the thrombin receptor in human
435 keratinocytes. Proc Natl Acad Sci U S A [Internet]. 1995 [cited 2025 Jun 21];92:9151–5.
436 Available from: /doi/pdf/10.1073/pnas.92.20.9151?download=true
437 24. Benito-Martínez S, Salavessa L, Raposo G, Marks MS, Delevoye C. Melanin Transfer
438 and Fate within Keratinocytes in Human Skin Pigmentation. Integr Comp Biol [Internet]. 2021
439 [cited 2025 Jun 21];61:1546–55. Available from: https://pubmed.ncbi.nlm.nih.gov/34021340/
440 25. Maurer M, Opitz M, Henz BM, Paus R. The mast cell products histamine and serotonin
441 stimulate and TNF-α inhibits the proliferation of murine epidermal keratinocytes in situ. J
442 Dermatol Sci [Internet]. 1997 [cited 2025 Jun 21];16:79–84. Available from:
443 https://pubmed.ncbi.nlm.nih.gov/9438912/
444 26. Cho KA, Kim HJ, Kim YH, Park M, Woo SY. Dexamethasone Promotes Keratinocyte
445 Proliferation by Triggering Keratinocyte Growth Factor in Mast Cells. Int Arch Allergy
446 Immunol [Internet]. 2019 [cited 2025 Jun 21];179:53–61. Available from:
447 https://pubmed.ncbi.nlm.nih.gov/30909282/
448 27. Dobre A, Nedelcu RI, Turcu G, Brinzea A, Struna I, et al. Multiple Keratoacanthomas
449 Associated with Genetic Syndromes: Narrative Review and Proposal of a Diagnostic
450 Algorithm. Am J Clin Dermatol [Internet]. 2024 [cited 2025 Apr 19];26:45. Available from:
451 https://pmc.ncbi.nlm.nih.gov/articles/PMC11742465/

452 **SUPPLEMENTARY MATERIAL**

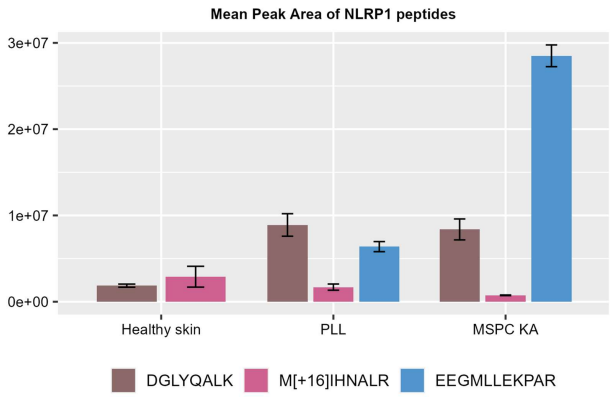

453

454 **Figure S1. Mean peak area of NLRP1 peptides identified by mass spectrometry.** Results
455 are presented as mean ± standard deviation (SD) for each peptide in healthy skin, psoriasis-like
456 lesion (PLL) and keratoacanthoma associated with multiple self-healing palmoplantar
457 carcinoma (MSPC-KA).

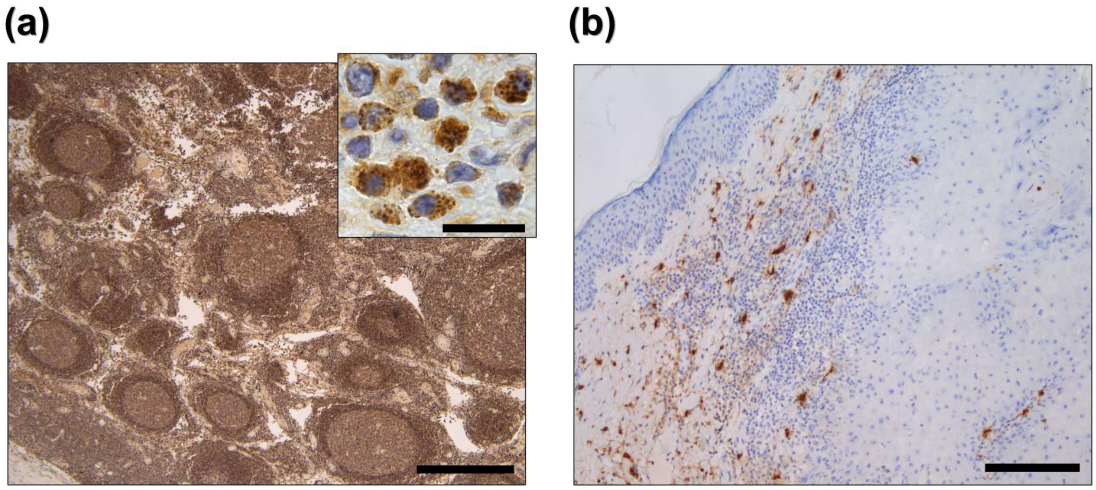

458

459 **Figure S2. Immunohistochemical analyses. (a)** Human lymph node stained against NLRP1,
460 showing highest proportion of positive cells in the mantle zone of lymphoid follicles. Scale bar
461 = 500 µm. Higher magnification **(inset**, scale bar = 20 µm**)** demonstrates localization of NLRP1
462 to granules of immune cells in lymph node. **(b)** Representative tryptase staining on KA from a

463 non-MSPC patient, showing absence of mast cell epidermal infiltration or degranulation. Scale
464 bar = 200 µm.

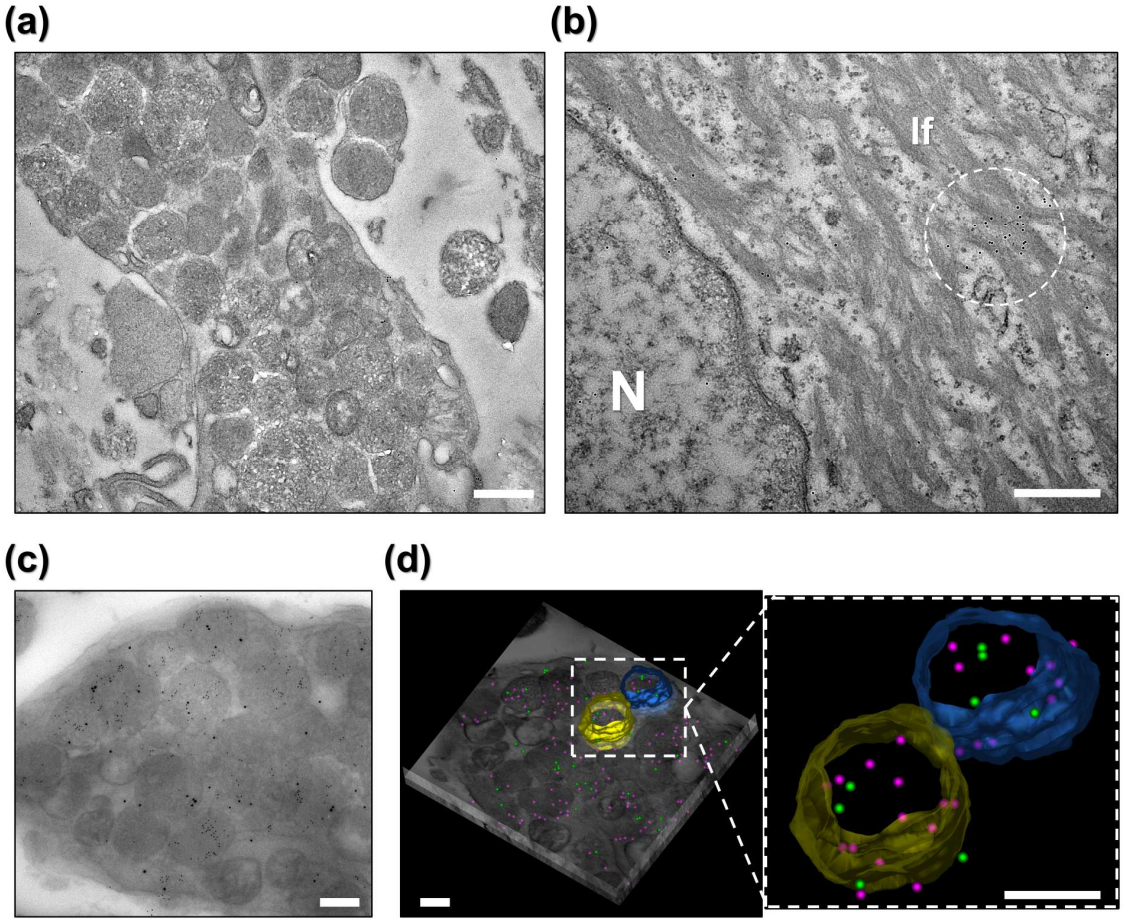

465

466 **Figure S3. Immunoelectron microscopy and tomography. (a)** A rabbit isotype control did
467 not significantly bind to mast cell (MC) granules. **(b)** NLRP1 localized to intermediate
468 filaments (If) of keratinocytes. Representative accumulation of colloidal gold can be seen as
469 black dots (circled area). *N - nucleus.* **(c)** Projection from tomographic tilt series, showing
470 colocalization of 10 and 15 nm gold particles ($NLRP1^{A66V}$ and NLRP3, respectively) in
471 granules from a MC in MSPC-keratoacanthoma. **(d)** Reconstructed tomogram with
472 superimposed drawn contours of two MC granules (yellow and blue), presenting colocalization
473 of $NLRP1^{A66V}$ (magenta) and NLRP3 (green). Detail of segmented MC granules demonstrating

474 colocalization of NLRP1^{A66V} (magenta) and NLRP3 (green) are presented in the boxed area.
475 Scale bars = 500 nm for (a-b) and 300 nm for (c-d).

476 **Table S1. Primary antibodies used for immunolabeling**

477 **Table S2. List of transitions for identified NLRP1 peptides.**

478 **Supplementary methods - mass spectrometry**

479 Biopsies were collected in cold PBS, then 50 mg from each sample was disrupted in a Mini-
480 Beadbeater (Biospec, US). Samples were then centrifuged for 20 minutes at 18,000 g and the
481 protein concentration from the supernatant was quantified by Bradford assay. A total of 50 µg
482 of protein containing supernatant was diluted with urea buffer to the final volume of 40 µL,
483 followed by the addition of 25 µL of 100 mM DTT and incubation at room temperature for 60
484 minutes. The sample was then alkylated with 26.25 µL of 300 mM iodoacetamide and kept in
485 the dark at room temperature for an additional 90 minutes followed by a quenching reaction
486 with 50 µL of DTT 100mM at room temperature for 60 minutes. The reaction mix was finally
487 diluted to 500 µL with 50 mM ammonium bicarbonate, followed by addition of trypsin (1 µg
488 /µL; Trypsin Gold, V528A, Promega, US) at a 1:50 enzyme-to-substrate ratio, with incubation
489 at 37°C for 16 hours. The reaction was stopped by adding 3 µL of formic acid. Peptides were
490 cleaned up using solid phase extraction (MonoSpin C18, GL Sciences, Japan), dried at speed-
491 vac and rehydrated to 2 µg/µL using 5% ACN + 0.1% HCOOH. Peptide concentration was
492 measured using NanoDrop 1000 (Thermo Fisher Scientific, US). From each sample, 5 µg
493 peptides were loaded into nanoACQUITY UPLC system (Waters, US) and separated using an
494 Eksigent 5C18-CL-120 (300 µM ID, 150 mm length) column coupled with a TripleTOF 5600+
495 mass spectrometer (both AB Sciex, USA). Peptide samples (5 µg) were injected using Solvent
496 A (0.1% formic acid) and separated on a 5-90% gradient Solvent B (0.1% formic acid in
497 acetonitrile) over 90 minutes, at a flow rate of 5 µL/min, with the column maintained at 55°C.

498 Each sample underwent three replicate runs. Mass spectrometric analysis was carried out using
499 electrospray ionization in positive mode, with a spray voltage of 5500 V and a source
500 temperature of 200°C. Data acquisition was performed on a TripleTOF 5600+ system in DIA
501 SWATH-MS mode, with 64 variable isolation windows. The MS1 survey scans covered an
502 m/z range of 400–1250, while MS2 spectra were collected in high-sensitivity mode from 100
503 to 2000 m/z. The accumulation period was set to 0.049 s, and ions were scanned within 55 ms
504 windows in high-sensitivity mode, giving a total cycle time of 3.5 s. Peptide and protein
505 identification were performed using PeakView 2.2, Skyline 22.2.0.255 and DIA-NN 1.9.

506 **Movie S1. NLRP1 and NLRP3 colocalize to MC granules in MSPC-KA.**

507 **Movie S2. NLRP1, NLRP3 and IL1β colocalize to MC granules in MSPC-KA.**